Distortion of atomic states by time-dependent electric fields. II. Coupling to the continuum

Predrag Krstić and Yukap Hahn
Physics Department, Box U-46, University of Connecticut, Storrs, Connecticut 06269
(Received 18 April 1994; revised manuscript received 27 June 1994)

The previously derived approximation for an atom in time-dependent electric fields [P. Krstić and Y. Hahn, Phys. Rev. A **48**, 4515 (1993)] is improved for electric pulses of both short and long duration. The transitions that involve a distorted continuum are studied in detail, and the phenomenon of momentum coherence is shown to greatly enhance the transition amplitudes. A detailed comparison with the recent experiment of Jones, You, and Bucksbaum [Phys. Rev. Lett. **70**, 1236 (1993)] is presented, where a half-cycle high-power laser pulse was used to ionize Rydberg atoms.

PACS number(s): 32.60.+i, 31.70.Hq

I. INTRODUCTION

Time-dependent fluctuations in plasma may be described, to lowest order, by a time-dependent electric field (TDF). This can modify numerous atomic processes that take place in the plasma environment [1–4]. Particularly sensitive to the TDF are the processes that involve high Rydberg states (HRS's) and a low-energy continuum. Recent experiments [5] on ionization of HRS atoms by a half-cycle pulse (HCP) as well as enhancement in radiative recombination [8] of very-low-energy electrons constitute grounds for testing the TDF effect on processes that involve both bound states and a continuum.

The previously derived approximation [1] for distortion of electronic wave functions $\Phi_{n_0}(\mathbf{r},t)$ in the central potential $V(r)$ and under the influence of a time-dependent electric field $\mathbf{F}(t)$ takes a simple form

$$\Psi'(\mathbf{r},t)=\exp[i\mathbf{g}\cdot\mathbf{r}-i\sigma(t)]\exp(-iH_A t)\phi_0(\mathbf{r}) , \tag{1.1}$$

where $\sigma(t)=\int_{-\infty}^{t}dt'g^2(t')/2$ and where $\mathbf{g}\equiv\mathbf{g}(t)=\int_{-\infty}^{t}\mathbf{F}(t')dt'$ is the momentum of an electron that moves classically with acceleration $\mathbf{F}(t)$ and $g=|\mathbf{g}|$. The subscript 0 denotes a particular initial state $j=0$, where $j=(n_j,l_j,m_j)$ is a set of quantum numbers of unperturbed atomic state $H_A\phi_j=E_j\phi_j$. The form given in Eq. (1.1) is an approximation to the initial-value problem $\Psi(\mathbf{r},t\rightarrow-\infty)=\exp(-iH_A t)\phi_0(\mathbf{r})$, as defined by the Schrödinger equation

$$[i\partial/\partial t-H_A+\mathbf{r}\cdot\mathbf{F}(t)]\Psi=0 . \tag{1.2}$$

The exact solution to this problem can be written in a form

$$\Psi(\mathbf{r},t)=\exp(i\mathbf{g}\cdot\mathbf{r})\exp(-iH_A t)\exp(-iX)\phi_0(\mathbf{r}) , \tag{1.3}$$

where $X(\mathbf{r},t)$ satisfies the operator equation

$$\begin{aligned}\partial X/\partial t&=g^2(t)/2-i\exp(iH_A t)\mathbf{g}\cdot\nabla\exp(-iH_A t)\\&=g^2(t)/2-i\mathbf{g}\cdot\nabla+[H_A,\mathbf{g}\cdot\nabla]t\\&\quad+(i/2)[H_A,[H_A,\mathbf{g}\cdot\nabla]]t^2+\cdots .\end{aligned} \tag{1.4}$$

The approximation (1.1) is obtained keeping only the $g^2/2$ term in the expansion (1.4), i.e., $X\cong\sigma(t)$. The neglected part of X is small for some values of the system and the field parameters. This is extensively tested in Ref. [1] and discussed later in this section.

If the exact wave function $\Psi(\mathbf{r},t)$ is expanded in the complete set of unperturbed eigenfunctions $\{\Phi_j(\mathbf{r},t)\}\equiv\{\exp(-iH_A t)\phi_j(\mathbf{r})\}$ as

$$\Psi(\mathbf{r},t)=\sum_j \alpha_j(t)\Phi_j(\mathbf{r},t) , \tag{1.5}$$

then Eqs. (1.2) and (1.5) with initial conditions $\alpha_j(t\rightarrow-\infty)=\delta_{j,0}$ yield a system of coupled differential equations. It was solved numerically, with different forms of time dependences for $F(t)$ [1,2]. The similar expansion of $\Psi'(\mathbf{r},t)$ of Eq. (1.1) gives

$$\begin{aligned}\alpha'(t)&=\exp[i(E_j-E_0)t-i\sigma(t)]\\&\quad\times\int d\mathbf{r}\,\phi_j^*(\mathbf{r})\exp[i\mathbf{g}(t)\cdot\mathbf{r}]\phi_0(\mathbf{r}) .\end{aligned} \tag{1.6}$$

The transition probabilities defined by the amplitudes in Eq. (1.4), $|\alpha_j'(t)|^2$, have been tested extensively by comparing them with the "exact" probabilities $|\alpha_j(t)|^2$ of Eq. (1.3), obtained from the large truncated basis of coupled hydrogenic states up to $n\leq 30$. The bounds of validity of (1.1) are discussed below. Comparison showed surprisingly good agreement for both the n and l,m mixing transition probabilities at different times t of the system evolution.

The probabilities $|\alpha_j'(t)|^2$ are shown to be a good approximation if the field-induced displacement $g\tau$ of the classical electron during the pulse duration τ is smaller than the wavelength $2\pi/v$ of the orbiting electron with velocity $v\sim 1/n_0$. If τ is small in comparison to the classical orbit period $T\sim 2\pi n_0^3$ of the initial state, this yields $gv\tau/(2\pi)\sim g\tau/(2\pi n_0)<1$. On the other hand, if $T<\tau$ and if the electron stays bound, the field-driven electron displacement does not exceed gT, which yields $gT/(2\pi/v)\sim gn_0^2<1$. For a continuum state $\Phi_q(\mathbf{r},t)$, the above discussion yields $g\tau q_c/(2\pi)<1$, where q_c is the classical electron momentum in the presence of $V(r)$, $q_c\cong[q^2-2V(r_c)]^{1/2}$, and r_c is an average distance of the

electron from the nucleus, which depends upon the process being studied. When $q \to 0$, a large Heisenberg uncertainty of r means large r_c and therefore small q_c. In effect, the dressing expressed in Eq. (1.1) becomes exact in the limit of small continuum momenta. On the other hand, Eq. (1.1) is also exact [1] in the limit $n_0 \to \infty$, yielding the smooth transition of the bounds of validity from large n_0 to the low-q continuum.

When $\tau > T$ and the velocity gain FT of the classical electron in an electric field $F = |\mathbf{F}|$ during the orbit time T is small enough so that the corresponding wavelength $1/(FT)$ is much larger than the characteristic dimensions of the atom $\langle r \rangle \sim n_0^2$, the system responds to the electric field adiabatically and transitions become possible only within the degenerated set of states of the initial n_0. The above condition is represented by the Inglis-Teller limit $\sim \frac{1}{3} F n_0^5 < 1$. The adiabaticity can be established also in the opposite limit $\tau \ll T$, when the wavelength of the electron gained in the filed pulse $2\pi/g$ is much larger than the characteristic dimension of the atom n_0^2, i.e., $g n_0^2/(2\pi) < 1$. Then, assuming that there is no n mixing of the states, an exact "adiabatic" solution to the field dressing problem can be derived [1,3], using the fact that the hydrogenic wave function in parabolic coordinates diagonalizes the electric dipole matrix element. It was shown by projecting both initial and final spherical states onto parabolic states that the wave function (1.1) is identical in the weak-field adiabatic limit to that obtained by the parabolic solution expressed in terms of the Clebsch-Gordan coefficients and linear Stark shift. Moreover, $\Psi'(\mathbf{r},t)$ in Eq. (1.1) is the exact solution to the problem Eq. (1.2) if the unperturbed Hamiltonian H_A is completely degenerate.

The numerical "experiments" reported in Ref. [1] were carried out for the bound states, neglecting the electric-field-induced coupling of the states to an atomic continuum. In most cases tested, transitions were localized in n to the neighborhood of n_0 of bound-state orbitals, while transitions involving an atomic continuum are difficult to test numerically. Rather than testing Eq. (1.1) directly, we consider applications of $\Psi'(\mathbf{r},t)$, and its improved forms (Sec. II), to processes that involve a continuum. In Sec. III the ionization probability is calculated and compared with experimental data for ionization of highly excited sodium atoms by a short half-cycle electric pulse [5] as well as with results of extensive classical and quantum-mechanical calculations of Reinhold *et al.* [6,7]. In addition, details of energy and the angular spectrum of photoelectrons are investigated. In Sec. IV radiative recombination of electrons with atomic ions in the presence of an external TDF is calculated. Large enhancement in the cross section is obtained, which may be relevant to the enhancements observed in recent experiments [8]. Our concluding remarks follow in Sec. V.

II. IMPROVEMENTS OF THE THEORY

Investigation of the $\alpha_j(t)$ and $\alpha_j'(t)$ (rather than corresponding probabilities) shows a discrepancy in the phases for $\tau < T$; the exact $\alpha_j(t)$ does not have time-dependent oscillations for large positive times $t \gg T > \tau$, while the $\alpha_n'(t)$ in Eq. (1.6) oscillate as $\exp[i(E_j - E_0)t]$. These phase are irrelevant in the calculation of transition probabilities induced by the field, but may be important when the approximate wave functions are used for a description of transitions induced by some other perturbation in the presence of the short electric-field pulses. To correct this situation we note that the ansatz

$$\Psi(\mathbf{r},t) = \exp[i\mathbf{g}\cdot\mathbf{r} - i\sigma(t)]\psi(\mathbf{r},t) , \tag{2.1}$$

where Ψ is the exact wave function of the Schrödinger equation (1.2), gives the equation for $\psi(\mathbf{r},t)$

$$(i\partial/\partial t - H_A + i\mathbf{g}\cdot\nabla)\psi = 0 . \tag{2.2}$$

If $F(t)$ is an odd function of time, we have $g(t > \tau) \to 0$. But if $F(t)$ is an even function (for example, a Gaussian pulse $F = F_0 \exp[-(t/\tau)^2]$), $g(t)$ shows a typical stepwise behavior, of the step "width" τ, as shown in Fig. 1. For $t > \tau$ (region 2) $g(t)$ is almost constant, $g(t > \tau) = g_0 = \int_{-\infty}^{\tau} F(t')dt'$. On the other hand, for time independent $\mathbf{g} = \mathbf{g}_0$ Eq. (2.2) can be solved exactly as

$$\psi_j(\mathbf{r},t) = \exp[-i\mathbf{g}_0\cdot\mathbf{r} + i(g_0^2/2)(t-\tau)] \times \exp[-iH_A(t-\tau)]\phi_j(\mathbf{r}) , \quad t \geq \tau , \tag{2.3}$$

where j spans all the quantum numbers of the unperturbed Hamiltonian H_A. Expanding $\psi(\mathbf{r},t)$ of Eq. (2.2) in ϕ_j, we have, for $\Psi(\mathbf{r},t)$,

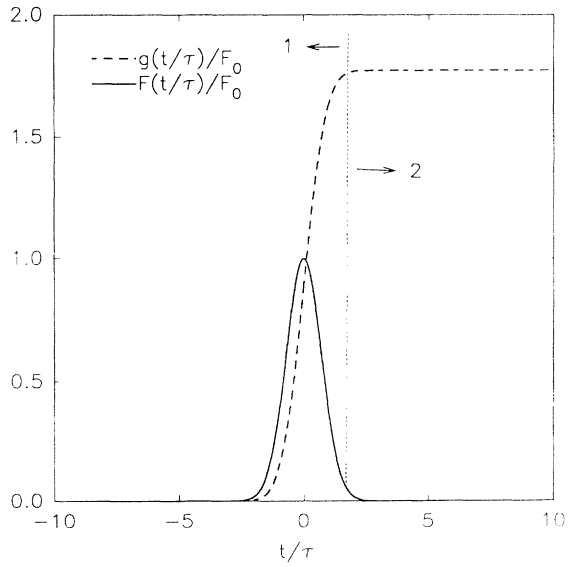

FIG. 1. The normalized Gaussian electric pulse $F(t/\tau)/F_0 = \exp[-(t/\tau)^2]$ (solid line) and the normalized field-induced momentum of a classical electron $g(t/\tau)/F_0 = \int_{-\infty}^{t} \exp[-(t'/\tau)^2]dt'$ (dashed line) are presented.

$$\Psi(\mathbf{r},t)\cong\exp[-i\sigma(\tau)]\sum_j C_j\exp[-iH_A(t-\tau)]\phi_j(\mathbf{r}) , \quad t\geq\tau , \tag{2.4}$$

where C_j are constant expansion amplitudes. Matching $\Psi'(\mathbf{r},t)$ of Eq. (1.1) with Ψ of Eq. (2.4) at $t=\tau$, we have, for C_j,

$$C_j=\exp(-iE_0\tau)\int d\mathbf{r}\,\phi_j^*(\mathbf{r})\exp(i\mathbf{g}_0\cdot\mathbf{r})\phi_0(\mathbf{r}) . \tag{2.5}$$

Finally, summing over the complete set $\{\phi_j\}$, the approximate wave function for the problem (1.2) may be written as

$$\Psi''(r,t)\cong\begin{cases}\exp[i\mathbf{g}\cdot\mathbf{r}-i\sigma(t)]\exp(-iH_At)\phi_0(\mathbf{r}), & t\leq\tau\\ \exp[-i\sigma(\tau)-iE_0\tau]\exp[-iH_A(t-\tau)]\exp[i\mathbf{g}(\tau)\cdot\mathbf{r}]\phi_0(\mathbf{r}) , & t\geq\tau .\end{cases} \tag{2.6}$$

The amplitude $\alpha_j''(t>\tau)$ of the expansion $\Psi''(r,t>\tau)=\sum_j\alpha_j''(t)\exp(-iH_At)\phi_j(\mathbf{r})$ is now equal to C_j, up to a constant phase, and does not oscillate with time. This was the desired behavior, as expected from the exact numerical solution.

Since $|\alpha_j'(t)|\equiv|\alpha_j''(t)|$, the transition probabilities induced solely by the electric field $\mathbf{F}(t)$ are not sensitive to the choice of the above approximate forms. When the transition is mediated by an external perturbation V' other than $\mathbf{r}\cdot\mathbf{F}(t)$, but in the presence of the field $\mathbf{F}(t)$, the corresponding amplitude may be sensitive to the modification introduced by Eq. (2.6).

When $F(t)$ is an odd function, the two approximations are identical $\Psi''(\mathbf{r},t)=\Psi'(\mathbf{r},t)$ and reestablish the initial state $\exp(-iE_0t)\phi_0(\mathbf{r})$ for $t>\tau$, the behavior that was also seen in the exact numerical solution [1].

According to the discussion given in the Introduction, the range of validity of $\Psi''(\mathbf{r},t)$ in Eq. (2.6) can be expressed as

$$\frac{g_0\tau}{2\pi n(1+\tau/T)}<1 \tag{2.7}$$

and this applies to cases of both "short" ($\tau<T$) and "long" ($\tau>T$) electric pulses [1].

As related to Eq. (2.6), we consider an alternate form of the wave function dressing by short electric-field pulses

$$\Psi'''(\mathbf{r},t)=\exp[-iH_A(t-t_0)]\times\exp[i\vartheta(t-t_0)\mathbf{F}_0\cdot\mathbf{r}]\phi_0(\mathbf{r}) . \tag{2.8}$$

$\Psi'''(\mathbf{r},t)$ is an exact solution of the initial value problem of Eq. (1.2) for $\mathbf{F}(t)=\mathbf{F}_0\delta(t-t_0)$, where $\delta(t)$ is the Dirac delta function and $\vartheta(t)$ is the unit step function. Assuming a finite $\tau\ll T$ of $F(t)$, with the ansatz

$$\Psi=\exp(-iH_At)\exp(i\mathbf{g}\cdot\mathbf{r})\psi' \tag{2.9}$$

in Eq. (1.2), the equation for $\psi'(\mathbf{r},t)$ can be written in the form

$$[i\partial/\partial t-H'(t)]\psi'=0 , \tag{2.10a}$$

where

$$H'=\mathbf{F}\cdot\mathbf{r}-\exp(-i\mathbf{g}\cdot\mathbf{r})\exp(iH_At)\mathbf{F}\cdot\mathbf{r}\times\exp(-iH_At)\exp(i\mathbf{g}\cdot\mathbf{r}) . \tag{2.10b}$$

Expanding formally

$$\exp(iH_At)\mathbf{F}\cdot\mathbf{r}\exp(-iH_At)=\mathbf{F}\cdot\mathbf{r}+i[H_A,\mathbf{F}\cdot\mathbf{r}]t-[H_A,[H_A,\mathbf{F}\cdot\mathbf{r}]]t^2/2+\cdots , \tag{2.11}$$

where

$$[H_A,\mathbf{F}\cdot\mathbf{r}]=-\mathbf{F}\cdot\nabla , \quad [H_A,[H_A,\mathbf{F}\cdot\mathbf{r}]]=\mathbf{F}\cdot\nabla V , \tag{2.12}$$

we get

$$\psi'\cong\psi^{(0)}(\mathbf{r},t)=\phi_0(\mathbf{r})\exp[i\sigma'(t)] , \tag{2.13}$$

where ϕ_0 is the initial atomic state and $\sigma'(t)=\int_{-\infty}^t dt't'F(t')g(t')$. The error introduced by $\psi^{(0)}$ is estimated from the matrix element of the next-order term

$$\Gamma_0(t)=\langle\phi_0\mathbf{h}(t)\cdot\nabla\phi_0\rangle\sim F_0\tau^2/n_0\sim F_0\tau^{2/3}(\tau/T)^{1/3} , \tag{2.14}$$

where $\mathbf{h}(t)=\int_{-\infty}^t dt't'\mathbf{F}(t')$ and F_0 is the field peak value. Note that $\psi^{(0)}$ contains $\sigma'(t)$, which is a part of the contribution of the term proportional to t in Eq. (2.11). Since $\partial\sigma'(t)/\partial t$ is proportional to $F_0\tau^2$, it belongs to zeroth-order term in the expansion of H' in powers of τ/T. The first order correction then gives

$$\psi^{(1)}(\mathbf{r},t)=\exp[i\sigma'(t)]\phi_0(\mathbf{r}+\mathbf{h}(t)) , \tag{2.15}$$

where the error is now

$$\Gamma_1(t)=\langle\phi_0\mathbf{w}(t)\cdot\nabla V_0(r)\phi_0\rangle\sim F_0\tau^2\tau/T \tag{2.16}$$

with

$$\mathbf{w}(t)=\int_{-\infty}^t dt'(t'^2/2)\mathbf{F}(t') . \tag{2.17}$$

Finally, the second-order approximation for ψ' is

$$\psi^{(2)}(\mathbf{r},t)=\exp[i\sigma'(t)]\exp[-i\mathbf{w}(t)\cdot\nabla V(\mathbf{r})]\phi_0(\mathbf{r}+\mathbf{h}) \tag{2.18}$$

with the error term

$$\Gamma_2(t)\sim F_0\tau^2(\tau/T)^2 \tag{2.19}$$

and so on. We note that if $F(t)$ is an even function of

time, then $h(\infty)=0$ and $\psi^{(1)}(\mathbf{r},t\to\infty)=\exp[i\sigma'(t\to\infty)]\phi_0(\mathbf{r})=\Psi^{(0)}(\mathbf{r},t\to\infty)$. Therefore

$$\Psi\sim\exp(-iH_A t)\exp(i\mathbf{g}\cdot\mathbf{r})\phi_0(\mathbf{r})\exp[i\sigma'(t)]\ ,\quad t\to\infty \tag{2.20}$$

is valid in the limit $t\to\infty$ if $F_0\tau^2\tau/T<1$. On the other hand, if $F(t)$ is an odd function, $g(\infty)=0$, $w(\infty)=0$, and

$$\Psi\sim\exp(-iH_A t)\phi_0(\mathbf{r}+\hbar)\exp[i\sigma'(\infty)]\ ,\quad t\to\infty \tag{2.21}$$

is the first nonvanishing approximation at $t\to\infty$, with error $\Gamma^2\sim F_0\tau^2(\tau/T)^2$.

When the electric field changes slowly on the atomic time scale T, the approximation (1.1) may be valid if the adiabaticity condition ($gn_0^2<1$) is fulfilled. We may improve Eq. (1.1) beyond this condition; the field-induced classical momentum $\mathbf{g}(t)$ does not take into account the feedback effect on $\mathbf{g}(t)$ of the field-induced dressing of the atom. When the field mixes various energy components of the wave function, the characteristic time of the mixing is limited to the period of the transitions $\tau_t\sim 1/\omega$, where ω is the frequency of transition; for bound states $\omega\sim 1/n_0^3\sim 1/T$. This partially restricts the effective time to $\tau_t<\tau$. We take this into account by replacing $\mathbf{g}(t)$ with $\mathbf{g}_{\rm res}(t)$, where

$$\mathbf{g}_{\rm res}(t)=\mathbf{g}(t)/(1+\tau/T)\ , \tag{2.22}$$

with $T=2\pi n_0^3$. The simplicity of Eq. (1.1) is preserved and we have

$$\Psi'_{\rm res}(\mathbf{r},t)=\exp[i\mathbf{g}_{\rm res}\cdot\mathbf{r}-i\sigma_{\rm res}(t)]\exp(-iH_A t)\phi_0(\mathbf{r})\ . \tag{2.23}$$

Since Eq. (2.22) specifically takes into account the effect of relative transition frequencies, those components of (2.22) associated with the states which are degenerate with $\phi_0(\mathbf{r})$ should not be modified. Thus $\Psi'_{\rm res}(\mathbf{r},t)$ is finally written as

$$\Psi'_{\rm res}(\mathbf{r},t)\to C\left\{\sum_{j\neq 0}\phi_j\rangle\langle\phi_j\exp(i\mathbf{g}_{\rm res}\cdot\mathbf{r})\phi_0\rangle\exp[-i\sigma_{\rm res}(t)]+\phi_0\rangle\langle\phi_0\exp(i\mathbf{g}\cdot\mathbf{r})\phi_0\rangle\exp[-i\sigma(t)]\right\}\times\exp(-iE_0 t)\ , \tag{2.24a}$$

where C is the field-dependent normalization factor

$$C=[1+|\langle\phi_0\exp(i\mathbf{g}\cdot\mathbf{r})\phi_0\rangle|^2-|\langle\phi_0\exp(i\mathbf{g}_{\rm res}\cdot\mathbf{r})\phi_0\rangle|^2]^{-1/2}\ . \tag{2.24b}$$

Note that, in Eq. (2.24a), the second term in large curly brackets contains the bare $\mathbf{g}$ and not $\mathbf{g}_{\rm res}$.

An application of Eq. (2.24) to the dressing of the bound states is shown in Fig. 2. The full line represents the field-induced l mixing transition probabilities within the set of hydrogenic states that are degenerate with initial state $(n_0,l_0,m)=(10,1,0)$. It is obtained by the solution of coupled equations with all hydrogenic states of zero magnetic quantum number m and all l and $n\leq 25$. The n mixing is expected to be insignificant in this case since $Fn_0^5<0.01$. Evidently, this is well represented by the exact numerical solution. For a given pulse duration τ, it follows that $g(\infty)=0.02$ and $gn_0^2=2$, and the wave function in Eq. (1.1) gives a spurious n mixing of about 50% (triangles in Fig. 2). On the other hand, the transition probabilities calculated from the wave function (2.24) contains almost no n mixing ($<0.02\%$) and the resulting l distribution (circles) almost coincides with the exact one. Another application of the dressed wave functions (2.23) and (2.24) is shown in the next section, where ionization of Rydberg atoms by a half-cycle electromagnetic pulse is considered.

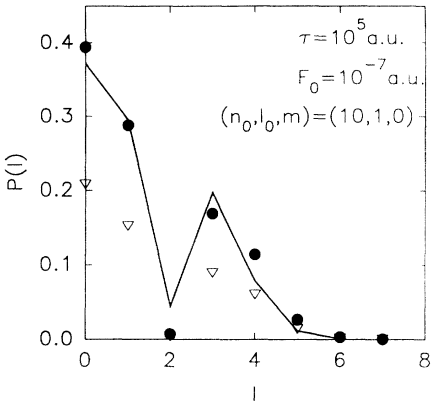

FIG. 2. The l-mixing transition probabilities induced by the adiabatically varying electric field $F(t)=F_0\exp(-|t|/\tau)$ are shown, where different wave functions are employed: "exact" numerical solution (solid line), approximate wave function of Eq. (1.1) (triangles), and wave functions of Eq. (2.24) (circles).

III. IONIZATION BY A HALF-CYCLE PULSE

In this section we test the proposed field-dressing formulas on a process that involves both bound and continuum states, i.e., ionization of high-Rydberg-state atoms by an electric pulse. The result is then compared with the experimental data of Jones, You, and Bucksbaum [5].

A half-cycle electric pulse was applied on sodium atoms, which were preexcited by two dye lasers to high Rydberg d states, of effective principal quantum numbers $n=15$, 20, and 35. The pulse $F(t)$ was approximately of triangular shape, with a half rise time of $\tau\cong 500$ fs. The exact S matrix for ionization into a final continuum state $\Phi_q^{(-)}(\mathbf{r},t)$ of momentum $\mathbf{q}$ can be written in the form

$$S_{\mathbf{q},0}=\lim_{t\to\infty}\langle\Phi_{\mathbf{q}}^{(0)}(\mathbf{r},t),\Psi_0^{(+)}(\mathbf{r},t)\rangle\ , \tag{3.1}$$

where $\langle\ \rangle$ means spatial integration and $\Psi_0^{(+)}(\mathbf{r},t)$ satisfies the exact Schrödinger equation of the problem Eq. (1.2) with the initial condition $\Psi_0^{(+)}(\mathbf{r},t\to-\infty)=\exp(-iE_0 t)\phi_0(\mathbf{r})$ and $\Phi_q^{(-)}(\mathbf{r},t)=\exp(-iE_q t)\phi_q^{(-)}(\mathbf{r})$. We approximate $\Psi_0^{(+)}(\mathbf{r},t\to\infty)$ by $\Psi''(\mathbf{r},t\to\infty)$ of Eq. (2.6), with appropriate modifications in Eqs. (2.22)–(2.24). The total ionization probability P_J is then given by the integral over $\mathbf{q}$

$$P_J=\int d\mathbf{q}|S_{\mathbf{q},0}|^2=C^2\int d\mathbf{q}|\langle\phi_{\mathbf{q}}\exp(i\mathbf{g}_{\mathrm{res}0}\cdot\mathbf{r})\phi\rangle|_0^2 , \quad (3.2)$$

where C is the normalization constant, defined by Eq. (2.24b), and $\mathbf{g}_{\mathrm{res}0}=\mathbf{g}_{\mathrm{res}}(\infty)=\mathbf{g}_{\mathrm{res}}(t>\tau)$. The initial and final atomic states are defined before the pulse is switched on and after it was switched off, respectively.

Although formally simple, actual calculation of the ionization probability by direct integration of (3.2) is difficult and numerically unstable for states with $n\geq 15$. The sum over all continuum states is therefore replaced by the complement of a semiclassical projection operator [9] which projects onto the subset of all hydrogenic bound states. It was given by

$$\begin{aligned}\Lambda_B &\equiv 1-\int d\mathbf{q}\,\varphi_{\mathbf{q}}^*(\mathbf{r}')\varphi_{\mathbf{q}}(\mathbf{r}) \\ &=\sum_j \varphi_j(\mathbf{r}')\varphi_j(\mathbf{r}) \\ &\cong[1/(2\pi^2u^3)][\sin(G)-G\cos(G)] , \end{aligned} \quad (3.3a)$$

where

$$G=(4/v)^{1/2}u , \quad u=|\mathbf{r}-\mathbf{r}'| , \quad v=|\mathbf{r}+\mathbf{r}'| . \quad (3.3b)$$

The ionization probability of Eq. (3.2) can now be written in the form $P_J=1-Q_J$, where Q_J, after averaging over magnetic quantum numbers of the initial state, is reduced to a three-dimensional integral

$$\begin{aligned}Q_J\cong\frac{1}{\pi}\int\int\int du\,dr'd\vartheta\sin(\vartheta)\frac{\sin(g_{\mathrm{res}0}u)}{g_{\mathrm{res}0}u} \\ \times\frac{[\sin(G)-G\cos(G)]}{u} \\ \times R_{nl}(|\mathbf{u}+\mathbf{r}'|)R_{nl}(r')P_l(x)\end{aligned} \quad (3.4)$$

and now $G=(4/|\mathbf{u}+2\mathbf{r}'|)^{1/2}u$, $x=(\mathbf{u}\cdot\hat{\mathbf{r}}'+r')/|\mathbf{u}+\mathbf{r}'|$, ϑ is the angle between $\mathbf{u}$ and $\mathbf{r}'$, and $P_l(x)$ with $x=\cos(\vartheta)$ is the Legendre polynomial arising from the angular dependence of the initial bound state of angular momentum l. The quantization axis is assumed in the direction of electric field. Since P_J involves high Rydberg states and continua, we neglected the sodium core, which is replaced by a hydrogenic model with minimal error. The operator Λ_B in Eq. (3.3a) can readily be improved using a model potential, if necessary [10,11].

The effectiveness of the approximate projection operator Eq. (3.3) is checked in two ways.

(i) In the limit $g_{\mathrm{res}0}\to 0$, the integral (3.4) is expected to be equal to 1 for any bound state (n,l). The calculated values are 0.99 for $(n,l)=5d$ and 0.997 for $(n,l)=10d$ and becomes numerically indistinguishable from the six-digit value of 1.000 00 for states with $n\geq 15$.

(ii) Calculation of the ionization probability from the state $(n,l)=(5,2)$ is done by direct integration Eq. (3.2) for a few values of $g_{\mathrm{res}0}$ (filled circles in Fig. 3) and using the projection operator Eq. (3.4) (hollow circles in Fig. 3). The agreement of the two calculations is excellent.

The field- and time-dependent energy shift $\sigma_{\mathrm{res}}(\tau)$, cumulated in the phase of the wave function for the pulse duration, does not influence the transitions between bound states, but can play an important role in bound-continuum transitions. The continuum threshold is effectively shifted downward by the value of classical kinetic energy $g_{\mathrm{res}}^2(t)/2$ gained by the electron in the electric field. We take into account this shift through the average value $\bar{\sigma}$ of $\sigma_{\mathrm{res}}(t)$ for the triangular pulse duration, defined as $\bar{\sigma}=\int_{-\tau}^{\tau}\sigma(t)dt/(2\tau)=(23/120)F_0\tau^2$. Then, Eq. (3.4) preserves its form, but with G redefined as $G=(-2\bar{\sigma}+4/v)^{1/2}u$. In the calculation of $g_{\mathrm{res}0}$ and $\bar{\sigma}$, the actual $F(t)$ was approximated by a triangle of the 1 ps base width and the height equal to the peak value F_0 of the pulsed electric field [5].

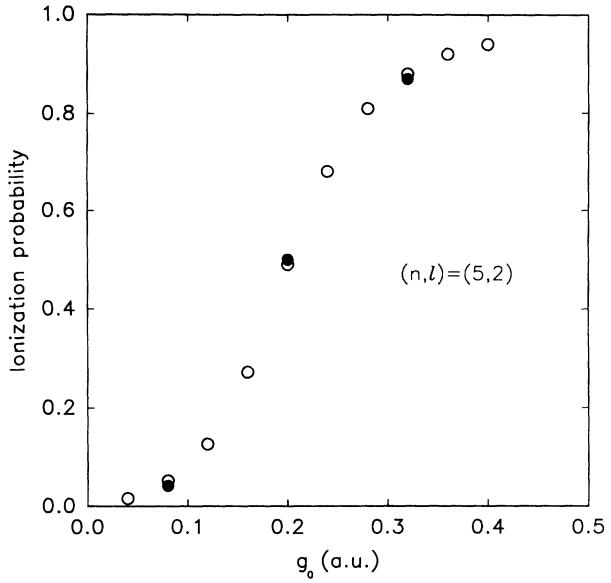

FIG. 3. Ionization probabilities from the state $5d$ of hydrogen are given. They are calculated using the semiclassical projection operator of Eq. (3.3) (hollow circles) and by the direct integration over all the final continuum states of Eq. (3.2) (filled circles).

We discuss the threshold behavior of the ionization probabilities as shown in Fig. 4. The effect of the energy exponent $\sigma_{\mathrm{res}}(t)$ in Eq. (2.23) is the shift of the continuum edge downward by a value of the kinetic energy $g_{\mathrm{res}}^2(t)/2$ gained by the electron in the electric field, where g_{res} is the reduced momentum transfer. Therefore, if the time of the pulse duration is τ, the ionization threshold is defined by $g_{\mathrm{res}}^2(\tau)/2=1/(2n^2)$, i.e., $g_{\mathrm{res}}=1/n$. Following the definition of $g_{\mathrm{res}}(t)$ Eq. (2.22), this yields

$$g(\tau)=1/n+(1/2\pi)\tau/n^4 . \quad (3.5a)$$

If one approximates $g(\tau)\cong F_0\tau$, where F_0 is the mean electric-field amplitude during the pulse duration, then Eq. (3.5a) is rewritten as

$$F_0=1/(n\tau)+(1/2\pi)1/n^4 . \quad (3.5b)$$

In the adiabatic limit ($\tau\to\infty$), this takes the well-known form of the classical field ionization threshold law $\sim 1/n^4$, with $1/(2\pi)$ in place of the classical $\frac{1}{9}$. In the

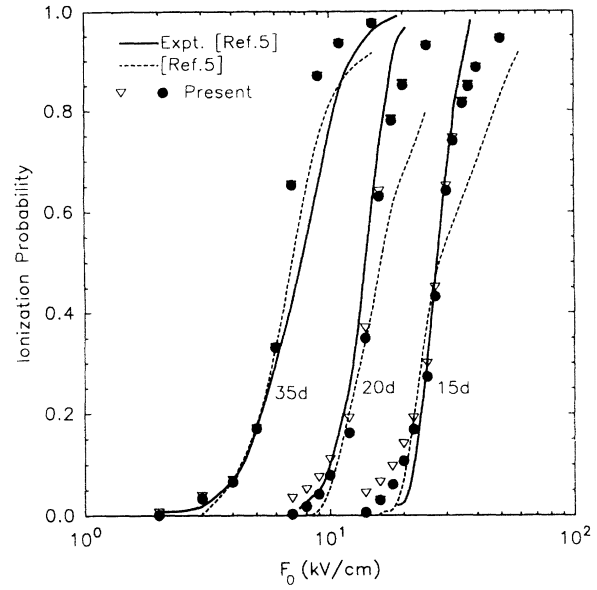

FIG. 4. The experimental ionization probabilities of Jones, You, and Bucksbaum [5] are compared with the theory: the effective hydrogenic states $15d$, $20d$, and $35d$ (solid lines); the full classical calculation in Ref. [5] (dashed lines); present calculation, using Eq. (2.23) (triangles) and Eq. (2.24) (hollow circles).

limit of short pulses, Eq. (3.5a) yields $g(\tau)=1/n$, which was obtained by Reinhold *et al.* [6] by extensive quantum-mechanical and classical calculations. The comparison of Eq. (3.5a) (solid line) with the result of Ref. [6] (symbols) is presented in Fig. 5. For 50% ionization threshold, the hollow circles show excellent agreement with Eq. (3.5a), while the 10% ionization threshold

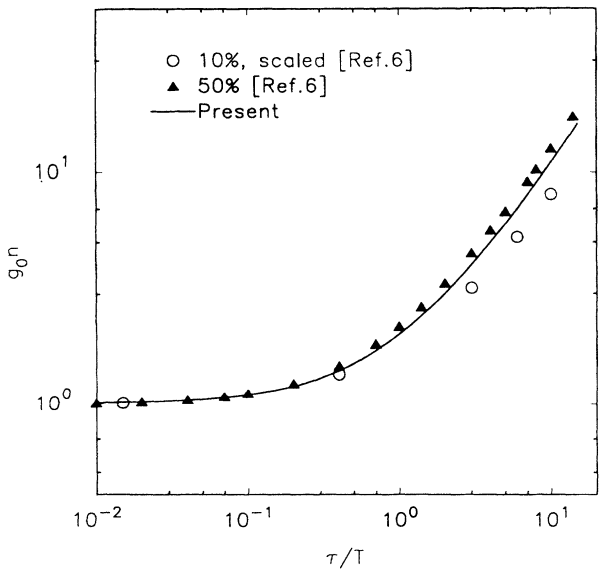

FIG. 5. The scaled total field momentum $g(\tau)n$ vs the scaled field pulse duration τ/T at the ionization threshold; solid line, Eq. (3.5a); circles, 50% ionization threshold, Ref. [6]; triangles, 10% ionization threshold, scaled by a factor of 0.54 of the result given in Refs. [5,6].

data of Ref. [5] (triangles) are shown after reducing them by a factor of 0.54. Therefore a formula for the ionization threshold induced by an electric field of an arbitrary duration may be written in the form

$$g(\tau)=c_1/n+(1/2\pi)c_2\tau/n^4 , \tag{3.6}$$

where parameters c_1 and c_2 depend upon the degree of ionization η and can be determined from extensive calculations in the "sudden" and adiabatic limit, as was done in Ref. [6]. Comparing with Eq. (3.5a), we have $c_1=c_2=1$. $c_1=1$ was obtained in Ref. [6] for $\eta=50\%$. For a classical threshold field in adiabatic limit $[1/(9n^4)]$, we obtain instead $c_2=0.7$ by fitting their data. On the other hand, for $\eta=10\%$ their result yields $c_1=0.54$. As pointed out by Reinhold *et al.* [6], the ionization threshold behavior $\sim 1/n^2$, which follows from the experimental results of Jones, You, and Bucksbaum [5], Fig. 4, may be interpreted as a form intermediate between the short pulse and adiabatic limit in Fig. 5.

Calculation of ionization probabilities using Eq. (3.4) and including the shift of the continuum edge gives the result shown in Fig. 4 (circles). The dashed lines are the classical calculations of Ref. [4]. The ionization probabilities were also evaluated using the wave function (2.23) (triangles). The increased probabilities near the ionization threshold, especially for $n_0=15$, may be due to a small spurious n mixing produced by $\Psi'(\mathbf{r},t)$ when $\tau \gtrsim T$, as discussed at the end of the Introduction and in Ref. [1]. The Inglis-Teller adiabatic limit $F_0 n_0^5/3 \cong 1$ gives for $n_0=15$ the limiting electric field $F_0=20$ kV/cm. This happens to correspond to the experimental threshold in Fig. 3. At the same time, $g_0 n_0^2/(2\pi)>1$ for $F_0<20$ kV/cm. The normalization constant C [Eq. (2.24b)] suppresses the spurious n mixing and thus improves the field dressed functions with the energies about the ionization threshold. On the other hand, $\tau \ll T$ when $n_0=35$ and the adiabatic limit [1] is defined by $g_0 n_0^2/(2\pi)\cong 1$. As long as $g_0\tau/(2\pi n_0)<1$ (which corresponds to $F_0<\sim 3$ kV/cm), the n mixing of the initial bound state is localized to a few neighboring states and ionization remains small. As seen in Fig. 4, the ionization curve for $n_0=35$ suddenly changes its slope when F_0 reaches 3 kV/cm.

Expressing $g_{\text{res}0}\equiv g_0/k$, we note that $k=1.07$ for $n_0=35$, $k=1.40$ for $n_0=20$, and $k=1.94$ for $n_0=15$. The modification introduced in Eq. (2.22) influences the location of the probability curves, shifting them toward higher F_0, but does not influence their slopes. This shift is negligible for the curve with $n_0=35$, while the effect of lowering the continuum edge $\bar{\sigma}(\tau)$ is sizable for this n_0. The $\bar{\sigma}(\tau)$ increases the slope of the curve at higher field intensities, causing the calculated values to diverge from the experimental data. We blame this discrepancy on the neglect of the second-order Stark shift α_0^S of the initial state, where α_0^S has opposite sign to $\bar{\sigma}(\tau)$ and is proportional to n_0^6. Its effect becomes significant for larger n_0. Our estimates show that α_0^s is almost negligible as compared to $\bar{\sigma}(\tau)$ for $n_0=15,20$, but becomes comparable in magnitude to $\bar{\sigma}(\tau)$ for $n_0=35$.

The field dressing of the system produces interesting

features in the energy spectrum and angular distribution of the photoelectrons. We show in Fig. 6 the qualitative features of the spectra for ionization by electric pulse from hydrogenic state $5d$, where the momentum (solid lines) and energy (dashed lines) spectra of the photoelectrons for three values of $g=g(\infty)$ are presented. They are defined as

$$\partial P_J/\partial q = q^2 \int d\Omega_q |\langle \phi_q \exp(i\mathbf{g}_0\cdot\mathbf{r})\phi_0\rangle|^2 ,$$
$$\partial P_J/\partial E_q = \partial P_J/(q\partial q) . \tag{3.7}$$

The peaks in the spectra are a consequence of the constructive interference of the factor $\exp(i\mathbf{g}_0\cdot\mathbf{r})$ and the continuum state $\phi_q^{(-)}(\mathbf{r})$. We call this the momentum coherence (MC) effect. This effect can be illustrated for a simplified case of a plane-wave final state $\phi_q(\mathbf{r})\cong\exp(i\mathbf{q}\cdot\mathbf{r})$. If the atom is ionized to a continuum state of momentum $\mathbf{q}$, the corresponding amplitude Eq. (3.2) is the largest when $\exp(-i\mathbf{q}\cdot\mathbf{r})\simeq\exp(i\mathbf{g}_0\cdot\mathbf{r})$. This produces peaks 2 and 3 in Fig. 6 [continuum-state momentum coherence (CSMC)]. On the other hand, for $q=0$ (zero-energy photoelectrons), the electron in the field of the parent ion has a classical momentum $q_c=\sqrt{-2V(r)}$, which produces slow oscillations in the zero-energy continuum wave function. When $g_0\cong 1/n_0$, this oscillation will again be partially canceled by the field dressing factor and an enhancement is produced in the energy spectrum [the bound-state momentum coherence (BSMC)]. Finally, when the electron is ionized with the final momentum $q=g_0-1/n_0$, the oscillations due to both q and q_c are canceled and give peak 1 in Fig. 3. For the curve with $g_0=0.2$, BSMC appears as the low-energy amplification in the energy spectrum, which coexists with the CSMC peak at $q=0.2$. For $g_0=0.1$ only the CSMC peak is visible in the momentum spectrum.

An expansion of the continuum state $\phi_q(\mathbf{r})$ into partial waves and averaging over the angles of the final momentum and initial magnetic quantum numbers yields the matrix element in Eq. (3.7) written in the form of a sum over radial integrals

$$\int dr\, r^2 R_{ql_c}(r) j_l(g_0 r) R_{n_0 l_0}(r) . \tag{3.8}$$

In Eq. (3.8) $j_l(g_0 r)$ is the spherical Bessel function. The momentum coherence is seen in the radial matrix elements through the constructive interference of the three oscillating functions in the integrand, as shown in Fig. 7(a) (solid line), for the CSMC peak 3 in Fig. 6. The integrands (dashed line) for the BSMC with $g=0.2$ and $q=0.05$ are also shown. In both cases the integrands are of definite sign, thus significantly increasing the amplitude. The squared matrix elements that correspond to Fig. 7(a) are shown in Fig. 7(b) as functions of q (CSMC) and in Fig. 7(c) as functions of g (BSMC). In producing the momentum coherence, the respective intrinsic phases also match up. That is, $\phi_c\cong\phi_g$, where $\phi_c=\beta_{l_c}-l_c\pi/2+\delta_{l_c}$ for the Coulomb and core phase shifts β and δ, respectively, and $\phi_g=-l\pi/2$ of the spher-

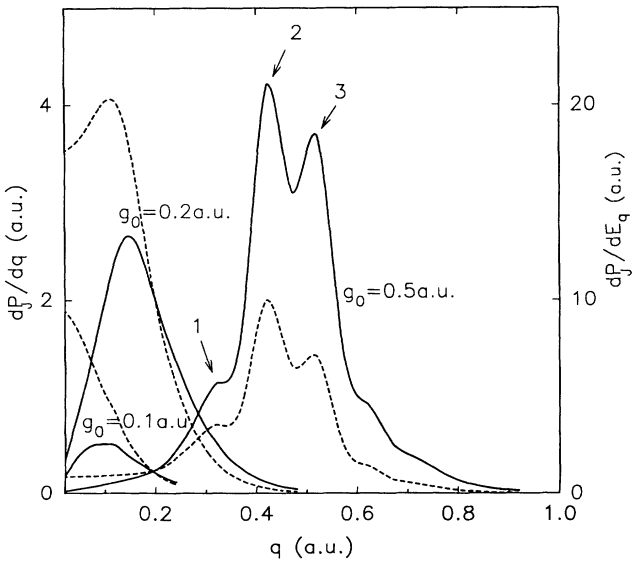

FIG. 6. The energy (dashed lines) and momentum (solid lines) spectra of electrons from ionization of the hydrogen state $5d$, for different values of g_0; the CSMC (2 and 3) and BSMC peaks (1).

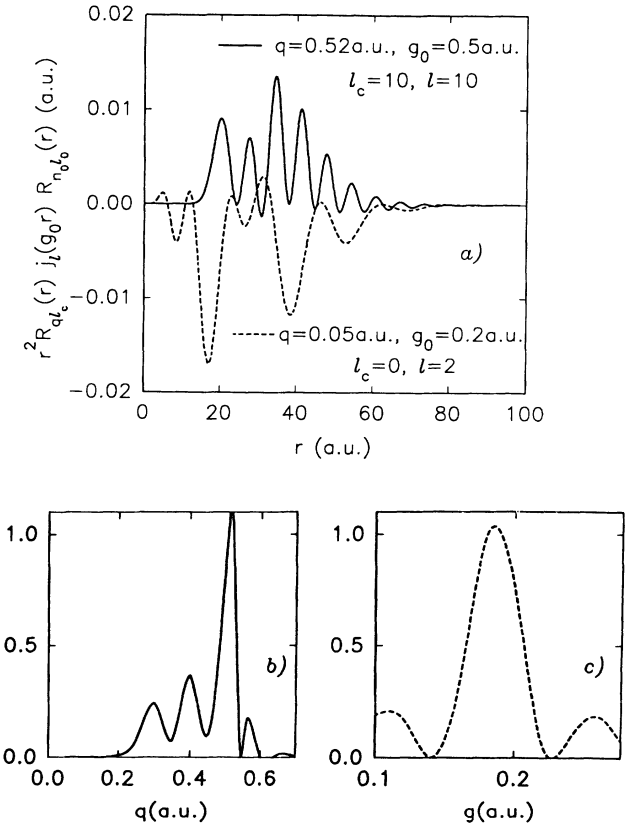

FIG. 7. The constructive interference in the continuum-bound dressed state radial matrix elements are illustrated: (a) integrand of CSMC (solid line) and BSMC (dashed line) matrix elements, for a selected set of values of q and g_0; (b) the CSMC matrix element with l_c, l, and g_0 as in (a) versus continuum momentum q; (c) the BSMC matrix element with q, l_c, and l as in (a) versus the "field" momentum g_0.

ical Bessel functions associated with the dressing. They can be arranged in different ways, thus broadening the MC peaks. This is illustrated in Fig. 6.

Many l_c's also take part in CSMC and the resulting peaks are the product of both increased radial matrix elements and multiplicity of the l_c. On the other hand, BSMC is restricted to a few angular components of continuum, around the value of the initial l_0. These features are clearly seen in the angular spectrum of photoelectrons in Fig. 8, where $\partial P_J/\partial[\cos(\vartheta)]$ versus $\cos(\theta)$ is presented. We have

$$\partial P_J/\partial[\cos(\vartheta)]=q^2\int d\varphi_q|\langle\phi_q\exp(i\mathbf{g}_0\cdot\mathbf{r})\phi_0\rangle|^2\ , \qquad \cos(\vartheta)=\hat{\mathbf{q}}\cdot\hat{\mathbf{g}}_0\ . \tag{3.9}$$

For BSMC of Figs. 8(a) and 8(c), the electron spectra have rich structures. The presence of the BSMC component in peak 3 of Fig. 6 contributes to the structure in Fig. 8(f). Typical angular spectrum of the CSMC is spread in the direction of the applied field [Fig. 8(b) and 8(e)]. The stronger the field the more arrowlike the angular distribution obtained, as seen in Figs. 8(d) and 8(e). The angular spectrum can thus be used to distinguish between the BSMC and CSMC peaks in the energy spectrum of photoelectrons.

IV. RADIATIVE RECOMBINATION IN THE PRESENCE OF AN ELECTRIC-FIELD PULSE

The MC effect is a consequence of the constructive interference in the matrix elements between the field dressing term $\exp(i\mathbf{g}\cdot\mathbf{r})$ and the continuum state or the high Rydberg state. Therefore, it is not specific to the ionization process, but rather common to all processes that involve oscillating wave functions. We explicitly evaluate a radiative recombination (RR) cross section as it is modified by the field [12]. The RR amplitude assumes the form

$$T_{bc}^{\mathrm{RR}}\propto\int dt\,\langle\tilde{\Psi}_b^{(-)}|\boldsymbol{\varepsilon}\cdot\mathbf{r}e^{i\omega t}|\tilde{\Psi}_c^{(+)}\rangle\ , \tag{4.1}$$

where $\boldsymbol{\varepsilon}$ is the polarization vector of an emitted photon, b and c denote the bound and continuum states, respectively, and the tilde stands for the field distorted states, with outgoing (+) or incoming (−) wave boundary conditions.

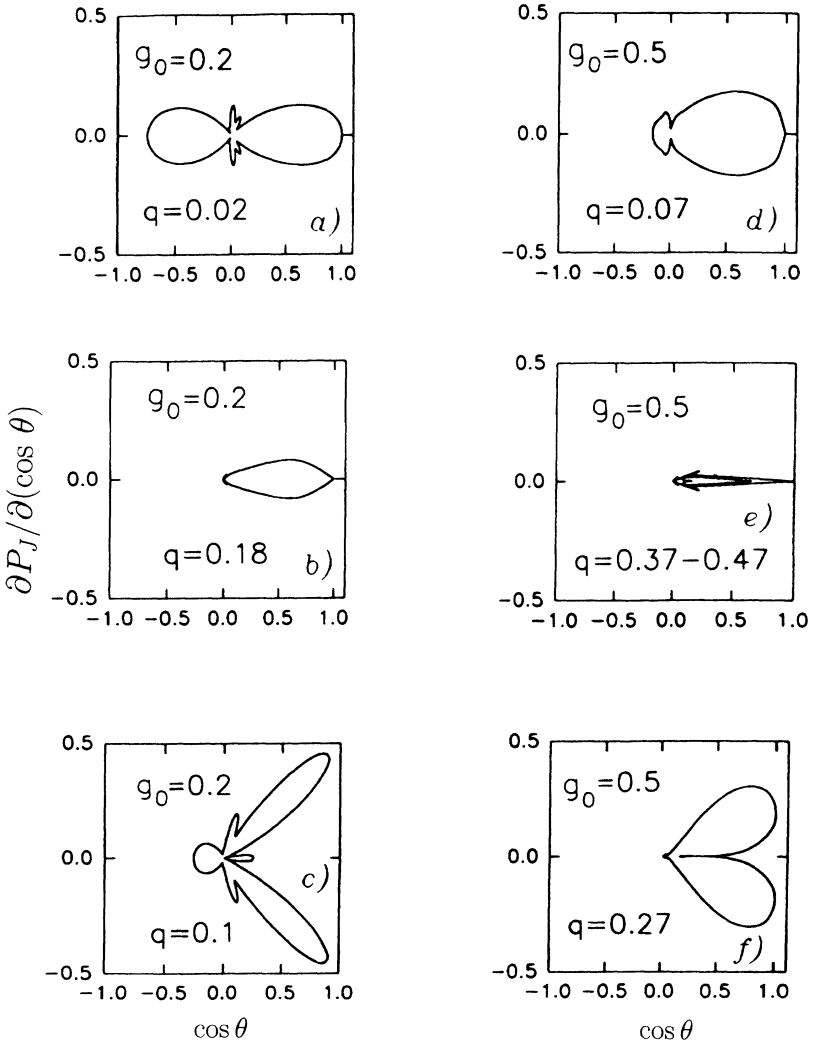

FIG. 8. Angular distributions of electrons as the result of ionization of state $5d$ by the field are given for various g_0 and q (in a.u.).

Using the field dressing (1.1) and neglecting the field-induced energy shift $\sigma(t)$, the dressed initial continuum state with outgoing boundary conditions takes the form

$$\Psi_c^{(+)} \cong \exp\left[i\int_{-\infty}^{t}\mathbf{F}(t')\cdot\mathbf{r}\,dt'\right]\phi_c(\mathbf{r})\exp(-iE_c t)\ . \quad (4.2)$$

The dressed final bound state with ingoing boundary conditions is then defined as a state that evolves in the electric field backward in time, starting from the bare bound state $\Phi_{nlm}(\mathbf{r})$ at $t=+\infty$. This yields

$$\Psi_b^{(-)} \cong \exp\left[i\int_{\infty}^{t}\mathbf{F}(t')\cdot\mathbf{r}\,dt'\right]\phi_{nlm}(\mathbf{r})\exp(-iE_n t)\ . \quad (4.3)$$

Replacing (4.2) and (4.3) in the S-matrix element in Eq. (4.1) yields exactly

$$T_{bc}^{\mathrm{RR}} \propto \int dt\,\langle\psi_b|\boldsymbol{\varepsilon}\cdot\mathbf{r}e^{i\mathbf{g}(\infty)\cdot\mathbf{r}}|\psi_c^{(+)}\rangle \times\exp[i(\omega+E_b-E_c)t]\ , \quad (4.4)$$

which (upon averaging over ω, $\boldsymbol{\varepsilon}$, and the incident electron directions and summing over the magnetic quantum numbers) yields the cross section

$$\sigma_{bc}^{\mathrm{RR}} \cong (8\pi^2/3q_c^2)\alpha_{fb}^3\Delta_{cb}^3 \times\sum_{l_c}(2l_c+1)\sum_{l}N(l_c,l,l_b) \times|\langle R_{bl_b}|rj_l(g_0 r)|R_{q_c l_c}\rangle|^2\ , \quad (4.5)$$

where α_f is the fine-structure constant, N is the usual angular factor in terms of the $3j$ symbols

$$N(l_c,l_b,l)=(2l_b+1)(2l+1) \times\left[(l_c+1)\begin{pmatrix} l_b & l & l_c+1\\ 0 & 0 & 0\end{pmatrix}^2 +l_c\begin{pmatrix} l_b & l & l_c-1\\ 0 & 0 & 0\end{pmatrix}^2\right]\ , \quad (4.6)$$

and $\Delta_{cb}=E_c-E_b$. In the limit $g\to 0$, we recover the unperturbed RR cross section.

The transition amplitude given by Eq. (4.4) contains the same form of the classical scaling law which is present in the ionization process and noticed before for processes with the Rydberg states [5,6]. Particularly, it shows that within the range of validity of approximation (1.1) the total momentum transferred by the field is an important quantity rather than the field at impact.

The actual length of the field pulse defines the bounds of the validity of approximation (1.1) and therefore the validity of the results in Sec. IV. Because of the scaling property of the cross section, the pulse duration need not be specified and can be defined later for the specific application.

On the other hand, inclusion of the energy shift $\sigma(t)$, as well as correction (2.22) to the definition of $g(\infty)$, would influence the ionization threshold in the problem, as defined by Eqs. (3.5). This would suppress the RR process when $g(\infty)$ is larger than the ionization threshold value and, depending upon the pulse duration, a part of the curves in the Fig. 9 could be unphysical.

The MC effect is here demonstrated through the momentum boost $\mathbf{g}$ of the continuum electron, and both CSMC ($\mathbf{g}=-\mathbf{q}$) and BSMC ($g=1/n$) maxima are obtained when the electron is slowed to almost zero energy. Similar coherence patterns, with large enhancement of the matrix elements as shown in Fig. 7, may also be shown for this case [12].

The RR cross section in the absence of the field σ_0^{RR} is calculated and compared with $\sigma_{bc}^{\mathrm{RR}}$ of Eq. (4.3). The enhancements, defined as $\sigma_{bc}^{\mathrm{RR}}(n_f)/\sigma_0^{\mathrm{RR}}(n_f)$ for $n_f=10$, are presented in Fig. 9 as a function of the incident electron momentum q. Very large enhancements, of $\sim 10^5$, are obtained for $g_0\equiv g(\infty)=0.2$ at the peak CSMC. The curve for $g_0=0.1$ shows the BSMC effect at lower momenta. In addition, the CSMC peak is also present at $q=0.1$.

A possible indication of the presence of this effect might have been seen in a recent experiment by Grimm, Schussler, and Muller [8], who observed an excessive number of soft photons in the RR experiment with very slow electrons. Detailed study of the BSMC effect in the total RR cross section and comparison with experiments will be given elsewhere.

V. DISCUSSION

The simple dressing procedure for atomic wave functions in a time-dependent electric field of arbitrary time dependence and orientation was developed in Ref. [1]. Its effectiveness is further demonstrated here in order to clarify the bounds of validity as well as to improve it without significant loss in simplicity. The improved wave functions in Sec. II are applied to cases of current experimental interest. The consequences of the dressing on the

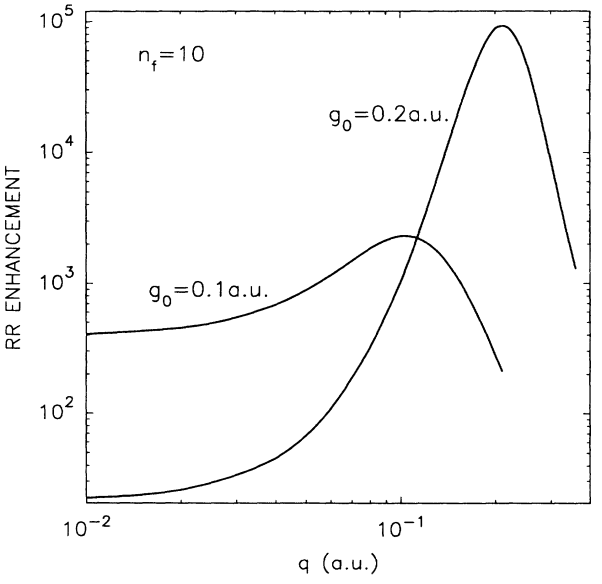

FIG. 9. The enhancement in the RR cross sections into the state with $n_f=10$ due to the MC effects, which is induced by g_0 of an electric-field pulse, as a function of the incident electron momentum q.

processes that involve atomic continuum and high Rydberg states have been studied in detail. As the first application, comparison with the experimental ionization probabilities of HRS by the HCP [5] is presented in Sec. III. Qualitative features of the energy and angular spectra of photoelectrons offer mechanisms for testing the MC effect experimentally. In addition, the large MC enhancements are obtained for the RR cross sections in the presence of an electric-field pulse. The MC mechanism as a possible explanation of the recent RR experiments is suggested.

ACKNOWLEDGMENTS

This work was supported in part by a grant from the Fundamental Interactions Branch, Division of Chemical Sciences, Office of Energy Research, Department of Energy. Discussions with Dr. G. Gibson on MPI were helpful.

[1] P. Krstić and Y. Hahn, Phys. Rev. A **48**, 4515 (1993).
[2] P. Krstić and Y. Hahn, Phys. Lett. A **192**, 47 (1994).
[3] Y. Hahn, and P. Krstić, J. Phys. B **26**, L297 (1993).
[4] Y. Hahn and P. Krstić, Phys. Scr. **48**, 340 (1993).
[5] R. R. Jones, D. You, and P. H. Bucksbaum, Phys. Rev. Lett. **70**, 1236 (1993).
[6] C. O. Reinhold, M. Melles, H. Shao, and J. Burgdorfer, J. Phys. B **26**, L659 (1993); C. O. Reinhold, M. Melles, and J. Burgdorfer, Phys. Rev. Lett. **70**, 4026 (1993).
[7] M. Melles, C. O. Reinhold, and J. Burgdorfer, Nucl. Instrum. Methods B **79**, 109 (1993).
[8] R. Grimm, T. Schussler, and A. Muller (unpublished) and private communications.
[9] Y. Hahn and K. M. Watson, Phys. Rev. A **6**, 548 (1972); **7**, 491 (1973).
[10] A. Z. Green, D. L. Sellin, and A. S. Zachov, Phys. Rev. **184**, 1 (1969); P. P. Szudlik and A. Z. Green, *ibid.* **9**, 1885 (1974).
[11] Y. Hahn, Phys. Rev. A **13**, 1326 (1976); Phys. Rev. Lett. **39**, 82 (1977).
[12] Y. Hahn and P. Krstić, J. Phys. B (to be published).